Received: 15 July 2024 | Revised: 20 August 2024 | Accepted: 23 August 2024

DOI: 10.1002/agt2.661

Aggregate WILEY Open Access

RESEARCH ARTICLE

Spin-coating fabrication of high-yield and uniform organic thin-film transistors via a primer template growth

Zhenxin Yang[1,2] | **Jiale Su**[1] | **Junzhan Wang**[3] | **Xuanhe Li**[1] | **Fushun Li**[1] | **Juntao Hu**[1] | **Nan Chen**[1] | **Zhang Tao**[1] | **Delong Yang**[2] | **Deng-Ke Wang**[1] | **Qiang Zhu**[1] | **Yuhui Liao**[2] | **Zheng-Hong Lu**[1,4]

[1]Key Laboratory of Yunnan Provincial Higher Education Institution for Optoelectronics Device Engineering, School of Physics and Astronomy, Yunnan University, Kunming, China

[2]Institute for Engineering Medicine, Kunming Medical University, Kunming, China

[3]Cavendish Laboratory, Cambridge University, Cambridge, UK

[4]Department of Materials Science and Engineering, University of Toronto, Toronto, Canada

Correspondence
Qiang Zhu and Zheng-Hong Lu, Key Laboratory of Yunnan Provincial Higher Education Institution for Optoelectronics Device Engineering, School of Physics and Astronomy, Yunnan University, Yunnan, Kunming, 650091, China.
Email: qiangzhu@ynu.edu.cn and zhenghonglu@utoronto.ca

Yuhui Liao, Institute for Engineering Medicine, Kunming Medical University, Yunnan, Kunming, 650500, China.
Email: liaoyh8@mail.sysu.edu.cn

Funding information
National Natural Science Foundation of China, Grant/Award Numbers: 62164012, 61904159; Applied Basic Research Foundation of Yunnan Province, Grant/Award Number: 202101AT070025

Abstract

Solution coating of organic semiconductors offers great potential for achieving low-cost and high-throughput manufacturing of large-area and flexible electronics. However, the solution processability of semiconducting small molecules for fabricating uniform and reliable thin-film devices poses challenges due to the low viscosities of small-molecule solutions. Here, we report a universal approach employing a primer template (PT) to enhance the spreadability of small-molecule solutions on silicon wafers, enabling the spin-coating fabrication of uniform thin films composed of millimeter-scale grains with complete large-area coverage and well-ordered molecular packing. Using PT, we fabricated organic thin-film transistors (OTFTs) using solutions containing various small molecules such as rubrene and 2-decyl-7-phenyl-[1]benzothieno[3,2-b][1]benzothiophene. The device yield of all fabricated OTFTs is consistently 100% while achieving a high average mobility of 1.62 $cm^2\ V^{-1}\ s^{-1}$ with a device-to-device variation of 7.7% measured in ambient air condition. In addition, the utilization of PT resulted in a batch-to-batch variation of 12.5% in device performance over dozens of OTFT devices. The key industrial manufacturing metrics, such as device yield, reproducibility, and performance uniformity of the PT OTFTs, are among the best for devices fabricated using solution spin-coating techniques.

KEYWORDS

device-to-device variability, film uniformity, organic semiconductors, solution process, thin-film transistors

1 | INTRODUCTION

Organic thin-film transistors (OTFTs) have emerged as a promising and cost-effective technology for the manufacture of flexible, large-area, and wearable electronics due to their high field-effect mobility and solution processability.[1–4] Recent advances in molecular design and synthesis of organic semiconductors (OCSs) have led to the development of materials with carrier mobilities surpassing that of amorphous silicon.[5–8] Compared to semiconducting polymers, small-molecule OSCs have been consistently achieving superior field-effect mobility in OTFTs, predominately utilizing single-crystal structures ranging from a few millimeters to even wafer scale.[9–11] However, the fabrication of single crystallized OCSs using either solution-based or vapor-based methods fails to meet the industrial requirements for continuous and high-throughput manufacturing due to issues such as inadequate crystal uniformity, challenges in precise positioning across a high density of devices, as well as instability and poor repeatability in the dynamics of crystal and film formation processes on substrates.[12–14] As a result, current efforts in organic electronics manufacturing lie in solution processing techniques, such as spin-coating, which facilitate the uniform deposition of large-area semiconducting organic thin films, thereby ensuring reproducible device performance.

Due to the low viscosity and dewetting nature of small-molecule solutions, achieving high coverage and uniform thin-film deposition on the substrate is challenging.[15] As a

result, attaining high device yield and uniformity in device performance poses formidable obstacles for OTFTs based on small-molecule OSCs. To overcome this challenge, recent studies focused on blending insulating binder polymers with small-molecule semiconductors in solution. The binder polymers, such as polystyrene, polymethylmethacrylate, and poly(alpha-methylstyrene), serve as effective thickening and wetting agents that can improve the thin-film morphology and uniformity of device performance over large areas.[16] In the blend film, the segregation of small-molecule semiconductors to the gate-dielectric interface is crucial for the performance of OTFTs. The presence of any binder polymers within the blend film located a few nanometers adjacent to the dielectric layer would significantly reduce carrier mobility due to their insulating nature and obstruction of small-molecular ordering and crystallization.[17] However, it is scarcely possible to completely avoid polymer residuals in the blend film near the dielectric layer. Therefore, the performance of small molecules is sacrificed when employing polymer blending. In addition to polymer blending, other techniques such as the epitaxial templating method and self-assembled monolayer modification are tried to manipulate the wetting behavior of small-molecule solutions on dielectric surfaces.[18–20] However, these techniques involve more complicated processes and achieving uniform templates and monolayers remains a challenge, resulting in inadequate device reproducibility. Moreover, the mismatch between molecular structures in templates or monolayers and small-molecule OCSs often induces disorder in adjacent OCS solid films. This not only degrades device performance, such as field-effect mobility and stability, but also triggers polycrystalline film formation leading to significant device-to-device variation.[21] Therefore, it would be preferable to avoid the utilization of these methods in industrial manufacturing.

Here, we proposed a primer template (PT) method for fabricating solution-processed OTFTs based on spin-coating. The PT layer, featuring a highly aligned grating-like topography, was deposited onto a silicon wafer through thermal evaporation of 2,2′,2″-(1,3,5-Benzinetriyl)-tris(1-phenyl-1-H-benzimidazole) (TPBi), followed by an annealing process. The utilization of TPBi-based PT significantly enhances the spreadability of small-molecule solutions on silicon wafers, thereby facilitating uniform and large-scale coverage of small-molecule films with millimeter-sized grains. In addition, the solubility of TPBi in solvents was controllable, allowing for the complete elimination of its doping effect in solution spin-coated films. Specifically, the rubrene-based OTFTs fabricated with the PT demonstrated a 100% device yield in the production of 90 devices and a significantly enhanced and uniform field-effect mobility (μ_{FET}), with variations of approximately 7.7% within a single-chip array of OTFTs and around 12.5% across different batches over dozens of devices. In comparison, the devices fabricated without PT or blending polymers exhibited a device yield lower than 44.4% and a significantly high CV exceeding 144.4% in a single-chip array. Additionally, the underlying mechanisms of PT-assistant OCS film formation were delineated, and the universal compatibility of the PT method in enhancing the electrical performance of OTFTs was demonstrated through spin-coating various OSC solutions. The OTFTs based on 2-decyl-7-phenyl-[1]benzothieno[3,2-b][1]benzothiophene fabricated with PT exhibited an average μ_{FET} of 1.62 $cm^2\ V^{-1}\ s^{-1}$ with variation of 8.6% measured in air condition, while the reference samples demonstrated a μ_{FET} of 0.44 $cm^2\ V^{-1}\ s^{-1}$ and CV of 93.2%, respectively. The OTFTs fabricated with PT surpass the previous records, such as consistently high mobility and minimal performance variability, achieved by spin-coating small-molecule solution on a silicon wafer, thereby rendering it potentially suitable for large-area industrial manufacturing.

2 | RESULTS AND DISCUSSION

Solution processing of OSCs plays a crucial role in attaining cost-effective fabrication of solid films and devices. However, conventional methods such as spin-coating are unsuitable for fabricating small-molecule-based OSC films and devices due to the low viscosities of solutions containing small molecules. In this work, a typical small-molecule OSC, rubrene, was chosen as the active layer material for fabricating OTFTs, serving as an illustrative example. A device configuration employing SiO_2/Si as the bottom gate and Ag source-drain electrodes as the top contact was utilized for the fabrication of the OTFTs. The process flow for device fabrication is depicted in Figure 1A. The rubrene film was deposited onto the SiO_2/Si substrate by spin-coating a 10 mg/mL solution of rubrene in 1,2-dichlorobenzene, followed by annealing under a nitrogen atmosphere. It is worth noting that prior to this study, we conducted an investigation into the impact of film annealing temperature on rubrene growth and device performance, revealing that annealing at 170°C yielded optimal p-type transistor behavior for rubrene-based devices due to the optimal topographic film structure. Based on these experimental findings, we selected an annealing temperature of 170°C for further investigation. Figure 1B illustrates the polarized optical microscopy (POM) image of the rubrene film directly deposited on the SiO_2/Si substrate. However, the rubrene film exhibits fragmented nature and incomplete coverage on the substrate, with a coverage ratio of less than 5% obtained on a 1.5 cm × 1.5 cm SiO_2/Si wafer substrate (Figure S1A). The transfer characteristics of the rubrene-based OTFTs (Rub-OTFTs) were measured subsequent to the deposition of Ag electrode arrays onto the rubrene film via the thermal evaporation method. The transfer curves of the Rub-OTFTs, recorded in ambient conditions at a source-drain voltage of −50 V, are depicted in Figure 2A, showcasing an OTFT array consisting of nine devices. It is observed that most of the OTFTs fail to function properly due to the fragmented nature of the rubrene film. The field-effect mobility (μ_{FET}) of the Rub-OTFTs operated at saturation region is calculated to be 0.09 $cm^2\ V^{-1}\ s^{-1}$. The standard deviation of the μ_{FET} of the Rub-OTFTs is 0.13 $cm^2\ V^{-1}\ s^{-1}$, indicating a significant device-to-device deviation, as shown in Figure 2E. The coefficient of variance (CV), which represents the ratio between the standard deviation and mean value of the μ_{FET}, reaches up to 144.4% for the Rub-OTFTs (Table 1). These results underscore the challenges encountered in fabricating small-molecule OSC films and devices through solution processing, particularly in attaining fully formed films with high coverage on the substrate.

To improve the quality of small-molecule OSC films prepared solution-based methods, a conventional polymer blending approach was employed in this work, where rubrene

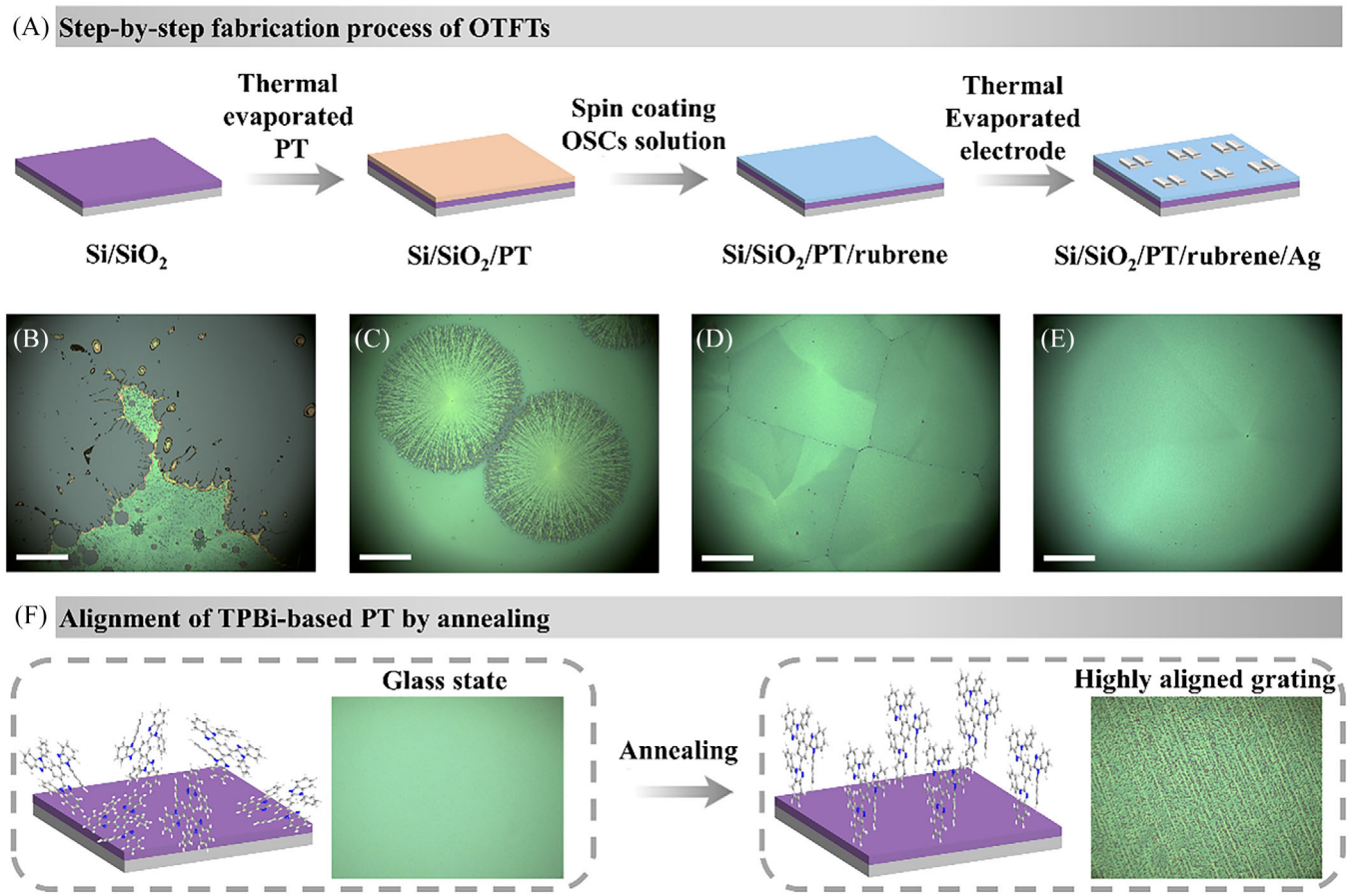

FIGURE 1 (A) illustrates the schematic step-by-step process of organic thin-film transistor (OTFT) fabrication. Images in (B–E) depict the polarized optical microscopy (POM) analysis of rubrene films fabricated using various spin-coating procedures, with scale bars indicating 500 um: (B) direct deposition of a rubrene film on SiO_2/Si substrate, (C) deposition of a rubrene/PS blend film on SiO_2/Si substrate, (D) deposition of a rubrene film on the SiO_2/Si substrate with primer template (PT), and (E) deposition of a rubrene film on the SiO_2/Si substrate with A-PT. (F) Depicts the transformation of 2,2′,2″-(1,3,5-Benzinetriyl)-tris(1-phenyl-1-H-benzimidazole) (TPBi) molecule orientation, alignment, and morphology following annealing treatment.

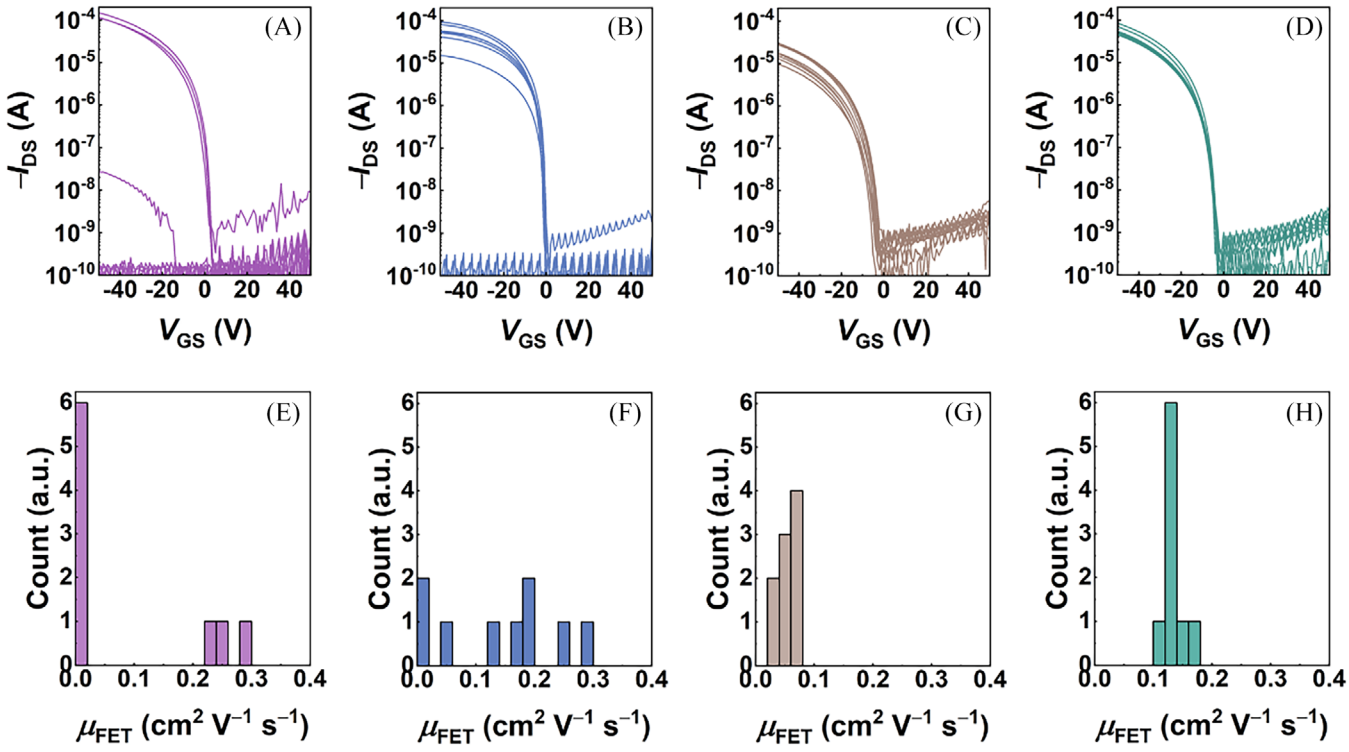

FIGURE 2 Transfer curves of (A) rubrene-based organic thin-film transistors (Rub-OTFTs); (B) Rub/PS-OTFTs; (C) PT/Rub-OTFTs; (D) A-PT/Rub-OTFTs. The corresponding histogram of field-effect mobility (μ_{FET}) of (E) Rub-OTFTs; (F) Rub/PS-OTFTs; (G) PT/Rub-OTFTs; (H) A-PT/Rub-OTFTs.

TABLE 1 Field-effect mobility (μ_{FET}), coefficient of variation (CV) in μ_{FET}, and device yield of organic thin-film transistors (OTFTs) fabricated using various methods.

OTFTs	μ_{FET} [$cm^2 V^{-1} s^{-1}$]	CV [%]	Device yield [%]
Rub-OTFTs	0.09 ± 0.13	144.4	44
Rub/PS-OTFTs	0.08 ± 0.05	62.5	77.8
PT/Rub-OTFTs	0.05 ± 0.02	40.0	100
A-PT/Rub-OTFTs	0.13 ± 0.01	7.7	100

and PS were blended in an optimized weight ratio of 4:1 using 1,2-dichlorobenzene as solvent for subsequent film deposition,[16] following the same processes employed for Rub-OTFT fabrication. Figure 1C and Figure S1B show the POM images of the rubrene/PS film deposited on the SiO_2/Si substrate, demonstrating an achievement of 100% film coverage ratio. However, a small fraction of spherulite grains were observed to be randomly dispersed in the film. To determine the aggregate state of these spherulite grains, the grazing incidence X-ray diffraction (GIXRD) analysis was performed, as depicted in Figure S2. The presence of a distinct diffraction peak suggests the crystalline nature of these grains. However, due to the rapid solidification kinetics and phase separation of PS from the rubrene solution, it impedes the diffusion of rubrene molecules, thereby leading to an inhomogeneous distribution of these crystalline spherulite grains in the film.[22] Figure 2B shows the transfer curves of the arrayed OTFTs based on rubrene/PS film (Rub/PS-OTFTs). The device yield of Rub/PS-OTFTs is significantly improved to 77.8%, in contrast to the Rub-OTFTs, where most devices fail to function properly, as indicated in Table 1. However, the Rub/PS-OTFTs show nonideal behavior (Figure S3A) and exhibit a dependence of μ_{FET} on gate voltage (V_{GS}) (Figure S3B). The μ_{FET} of the Rub/PS-OTFTs was determined using the reliability factor method.[23] The calculated μ_{FET} is 0.08 $cm^2 V^{-1} s^{-1}$, which is lower than that of the Rub-OTFTs. Additionally, the Rub/PS-OTFTs still show a large device-to-device deviation (Figure 2F), with a high CV of 62.5%. These results indicate that the phase separation of insulating PS from the blends, followed by the growth of spherulite grains in various orientations, leads to inferior and no-uniform electrical performance of OTFTs.

In addition to polymer blends, the template method presents an alternative approach for enhancing the quality of small-molecule films during solution processing. However, incorporating a template layer between the dielectric and OCS film compromises the gate controllability on the OCS film, rendering it unsuitable for OTFT fabrication. In this work, a PT method was proposed, in which solution-compatible small molecules were utilized as the PT materials to fine-tune characteristics at the solid/solution interface. The PT materials can be dissolved after the solution-based OCS film deposition, thereby effectively eliminating interference caused by the PT layer between the SiO_2 dielectric and OCS film. We investigated various organic materials for the PT fabrication and discovered that only 2,2′,2″-(1,3,5-Benzinetriyl)-tris(1-phenyl-1-H-benzimidazole) (TPBi) can effectively form a complete rubrene film while also exhibiting suitable solubility in 1,2-dichlorobenzene. Therefore, TPBi was chosen as the PT material for the device fabrication and subsequent investigation in this work. The TPBi PT was deposited onto the SiO_2/Si substrate using the thermal evaporation method, followed by direct spin-coating of the rubrene solution onto the TPBi PT for subsequent annealing and device fabrication, as illustrated in Figure 1A. The investigation covered the thicknesses of the TPBi PT ranging from 5 to 50 nm, with consistent findings that the TPBi PT of 30 nm always exhibited the highest film quality. Therefore, the present work focuses solely on the results obtained from a 30 nm TPBi PT. The POM images in Figure 1D and Figure S1C show the complete coverage of rubrene film on the SiO_2/Si substrate with TPBi PT, exhibiting uniform grain distribution throughout. The size of these grains was measured to be approximately 3 mm^2. The GIXRD pattern of the film is shown in Figure S2, revealing the absence of distinct diffraction peaks and indicating the amorphous nature of these grains composed of the film. The OTFT arrays were fabricated using the rubrene films deposited on the TPBi PT, denoted as PT/Rub-OTFTs. As shown in Figure 2C, all of the PT/Rub-OTFTs show the typical transistor behavior, with a device yield of 100%, surpassing both Rub-OTFTs and Rub/PS-OTFTs (Table 1). In addition, the PT/Rub-OTFTs demonstrate a reduced device-to-device variation in electrical performances with a CV in μ_{FET} of 40.0%. However, the mean μ_{FET} of the PT/Rub-OTFTs is 0.05 $cm^2 V^{-1} s^{-1}$, which is inferior compared to both Rub-OTFTs and Rub/PS-OTFTs (Table 1). This is because the solubility of TPBi in 1,2-dichlorobenzene leads to the doping of TPBi into the rubrene film (as evidenced by a faint N 1s peak observed from the XPS spectrum in Figure 3C), which impedes the molecular ordering of rubrene during the film annealing due to the increased steric bulkiness of TPBi compared to rubrene.[24] Due to the glass-forming nature of TPBi, the TPBi PT deposited by direct thermal evaporation exists in a glass state with high entropy, facilitating its facile dissolution into the solution. In addition, the glass state of TPBi is not conducive to induced molecular ordering in the rubrene films. Therefore, the PT/Rub-OTFTs exhibit suboptimal electrical performance in μ_{FET}.

To address the aforementioned issues, the as-deposited TPBi PT was subjected to annealing, denoted as A-PT, to enhance the molecular orientation and reduce the entropy of the PT. As shown in Figure 1F, the annealed A-PT underwent a remarkable transformation into a highly aligned grating-like topography compared to the initially deposited PT with a smooth surface morphology. To assess the molecular orientation of TPBi in the A-PT, the molecular orientation parameter (S) was evaluated by calculating using variable angle spectroscopic ellipsometry (VASE) determined extinction coefficients,[25,26] as illustrated in Figure S4. The as-deposited PT exhibited an S value of −0.10, while the annealed A-PT showed an S value of 0.15. As described in a previous study,[27] $S = -0.5$ if the molecules are parallel to the substrate surface, $S = 0$ if the molecules are randomly oriented, and $S = 1$ if the molecules are aligned perpendicular to the substrate surface. The result indicates that the annealing treatment resulted in the transformation of the disordered arrangement of TPBi parallel to the SiO_2/Si substrate surface into a well-aligned perpendicular orientation, suggesting an enhanced molecular ordering alignment of the A-PT as well as a reduction in entropy. The improved TPBi ordering is beneficial for the subsequent formation of rubrene films using a solution-based process and prevents

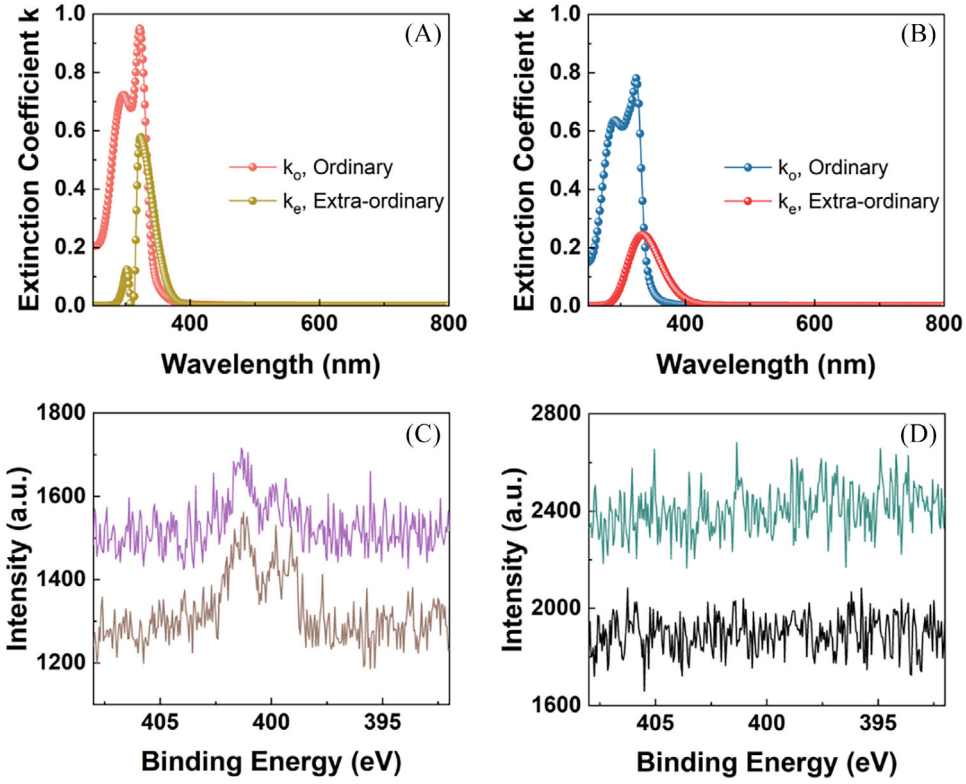

FIGURE 3 Extinction coefficients of rubrene films deposited on SiO_2/Si substrates with (A) primer template (PT) and (B) A-PT. N1s XPS spectra of rubrene films deposited on SiO_2/Si substrate with (C) PT and (D) A-PT. (The XPS signals recorded from the rubrene film surface are depicted by light violet and dark cyan curves in (C) and (D), respectively. The XPS signals obtained from the rubrene/SiO_2 interface by detaching the film from the substrate using 3 M adhesive tape are represented by dark brown and black curves in (C) and (D), respectively.)

TPBi dissolution. The rubrene film was deposited onto the A-PT using the same spin-coating procedure as that used for the PT device fabrication. Figure 1E illustrates POM images of the rubrene film deposited on the SiO_2/Si substrate with an A-PT layer, showcasing the larger-sized grains with a uniform morphology. The average grain size in the rubrene film is calculated to be 15 mm^2, and the largest grain area is up to 25 mm^2, as shown in Figure S1D. In addition, the rubrene grains deposited using the A-PT exhibit a more uniform intragrain color compared to those deposited using the PT with color gradients. It indicates the consistent orientation of rubrene molecules in the film deposited using the A-PT. To confirm the aggregate state of rubrene molecules in the grains, the GIXRD analysis was performed, as depicted in Figure S2. However, there is still no distinct diffraction peaks can be observed, indicating the amorphous nature of these rubrene grains. The uniform intragrain color can be attributed to the short-range ordering of rubrene molecules rather than crystallization. To determine the orientation of rubrene molecules in the films was investigated using the VASE. The S values of rubrene in the films deposited using the PT and the A-PT were determined to be −0.10 and −0.30, respectively, based on the extinction coefficients obtained from VASE measurements (as shown in Figure 3A,B). The results suggest that the solution-processed rubrene exhibits a preference for in-plane packing parallel to the substrate. The well-aligned A-PT can serve as nucleation sites for the heterogeneous nucleation growth of rubrene, leading to an enhanced parallel ordering and a significantly larger grain size of rubrene. In addition, the doping effect of TPBi was investigated by recording the XPS signals from both the rubrene film surface and the rubrene/SiO_2 interface, as depicted in Figure 3D, in which no N XPS signals were detected. This suggests that the annealing treatment on the A-PT can diminish the solubility of TPBi, consequently enabling the spontaneous removal of TPBi during the solution spin-coating procedure, and thus the subsequent doping effect in the rubrene films can be mitigated. On the other hand, the spontaneous removal of TPBi results in a decrease in the density of TPBi nuclei, thereby reducing the density of rubrene grains and leaving more space for the unhindered growth of rubrene grains. As a result, the rubrene film deposited on the SiO_2/Si substrate with the A-PT layer exhibits a significantly larger grain area.

Since the deposition of rubrene film using the A-PT offers several advancements, including larger-sized grains, ordered molecular orientation, and elimination of TPBi doping, the utilization of A-PT is expected to significantly enhance the electrical performance in OTFTs. Accordingly, the OTFT array based on the rubrene film with the A-PT (denoted as A-PT/Rub-OTFTs) was fabricated. As illustrated in Figure 2D, the transistor characteristics of all devices demonstrate a high electrical uniformity, resulting in a device yield of 100%. In comparison to Rub/PS-OTFTs with non-ideal behavior, the A-PT/Rub-OTFTs demonstrate a μ_{FET} independence on V_{GS}, as shown in Figure S3D. The mean μ_{FET} of the A-PT/Rub-OTFTs was calculated to be 0.13 $cm^2\ V^{-1}\ s^{-1}$, as listed in Table 1, which is nearly three times higher than that of the PT/Rub-OTFTs and comparable to the best record achieved by spin-coating method for the rubrene OTFT fabrication, surpassing the thermal evaporation-based rubrene film OTFT with a mobility of $10^{-4}\ cm^2\ V^{-1}\ s^{-1}$.[28] Notably, the A-PT/Rub-OTFTs exhibit superior device-to-device

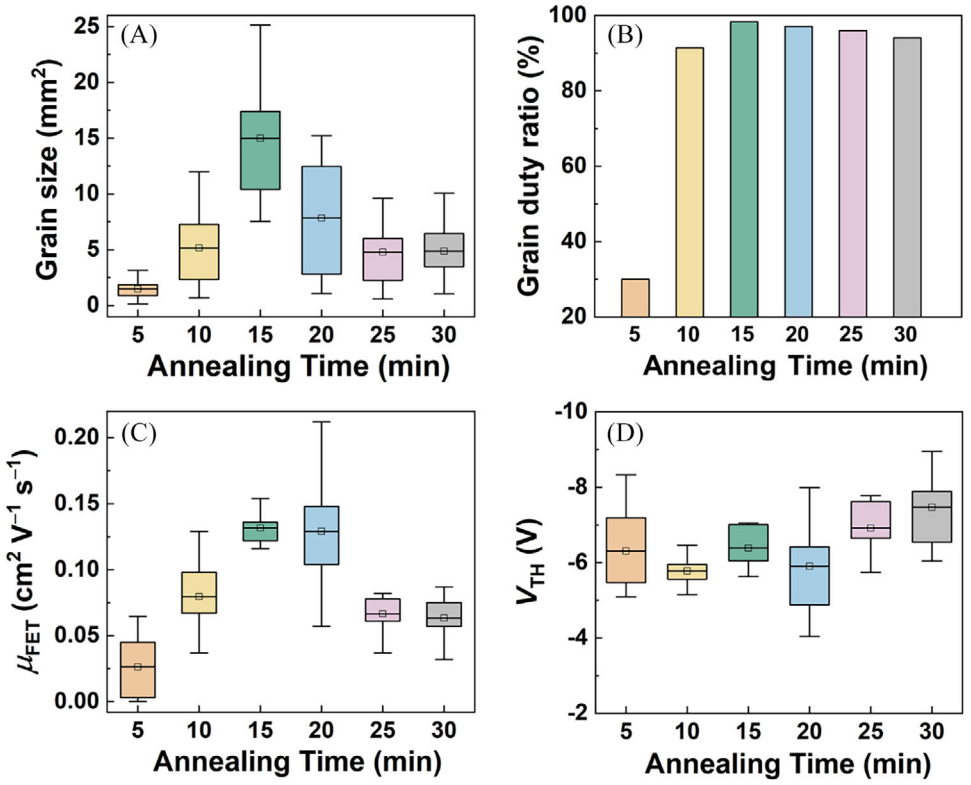

FIGURE 4 Statistical analysis on (A) size and (B) duty ratio of rubrene grains by varying annealing time of 2,2′,2″-(1,3,5-Benzinetriyl)-tris(1-phenyl-1-H-benzimidazole) (TPBi) primer template (PT). Statistical analysis on (C) field-effect mobility (μ_{FET}) and (D) threshold voltage (V_{TH}) of organic thin-film transistors (OTFTs) fabricated with the TPBi PTs annealed for different durations.

uniformity, characterized by a narrow distribution of μ_{FET} (Figure 2H). The CV in μ_{FET} of the A-PT/Rub-OTFTs is merely 7.7%, significantly lower than the value of 40.0% for the PT/Rub-OTFTs as well as the value of 8.9–56.6% achieved using other solution coating techniques listed in Table S1,[29–38] and it even outperforms the industry standard set for low-temperature polycrystalline silicon TFTs (8%–10%).[39,40] To further demonstrate the reproducibility of the OTFTs, we fabricated a total of 90 transistors divided into 10 batches for evaluation. The A-PT/Rub-OTFTs demonstrated excellent reproducibility, exhibiting a high mean μ_{FET} of 0.12 $cm^2\ V^{-1}\ s^{-1}$ and a CV of 12.5% across different batches (Figure S5). In contrast, the PT/Rub-OTFTs displayed a mean μ_{FET} of 0.05 $cm^2\ V^{-1}\ s^{-1}$ with a CV of 39.3%. Benefiting from the advancement in the A-PT method, the device performance of the A-PT/Rub-OTFTs is guaranteed to meet the industry requirements.

The growth mechanism of rubrene film using the A-PT was further investigated to gain insights into the behaviors of the OTFTs by controlling the annealing conditions. Figure S6 presents POM images of rubrene films with varying annealing times at 170°C. The grain size and the grain duty ratio in the rubrene films were analyzed based on the POM images, as summarized in Figure 4A,B. Upon annealing for 5 min, the platelet grains were observed in the film (Figure S6A). However, only a small portion of the film was covered by the grains. The average grain size was calculated to be 1.5 mm^2, and the duty ratio of the grains in the film was determined to be merely 30%. With an increase in the annealing time, the diffusion of rubrene molecules is enhanced. Consequently, smaller grains are gradually eroded by larger grains through a subcrystalline nibbling mechanism.[41] During this process, small grains disappear while large grains experience slow growth, resulting in a corresponding increase in the grain duty ratio (Figure S6B). After annealing for 15 min, an optimized grain size of 15 mm^2 and a grain duty ratio of 98% were achieved (Figure S6C). However, with a further increase in annealing time exceeding 15 min, the rubrene film undergoes degradation, characterized by the formation of a significant number of topographic defects within the grains (Figure S6D–F), accompanied by an expansion in the width of the crevices between adjacent grains (Figure S7). The observed degradation of the rubrene film can be attributed to a significant reduction in the viscosity of the rubrene solid above its glass transition temperature due to the absence of TPBi doping in the rubrene film when deposited using A-PT. Consequently, prolonged annealing induces molecular aggregation and film distortion to minimize interfacial energy between the rubrene film and substrate. Due to the expansion of grain boundaries and the aggregation of molecules during long-term annealing, the grain size decreases significantly, and the grain duty ratio on the substrate decreases as well. In addition, the films exhibited distinct intragrain color gradients following long-term annealing, which serves as evidence for molecule aggregation and realignment. This results in anisotropy both in the micro-structure and electric performances of the rubrene films and devices. As shown in Figure 4C, the OTFTs fabricated using the rubrene film with annealing for 5 min exhibit the lowest mean μ_{FET} of 0.03 $cm^2\ V^{-1}\ s^{-1}$ and an inferior CV of 92.6% due to discontinuous grain coverage. However, by increasing the annealing time to 15 min, the OTFTs demonstrate the highest mean μ_{FET} of 0.13 $cm^2\ V^{-1}\ s^{-1}$ and the lowest CV of 7.7% owing to maximum grain size and uniform grain coverage. The electrical

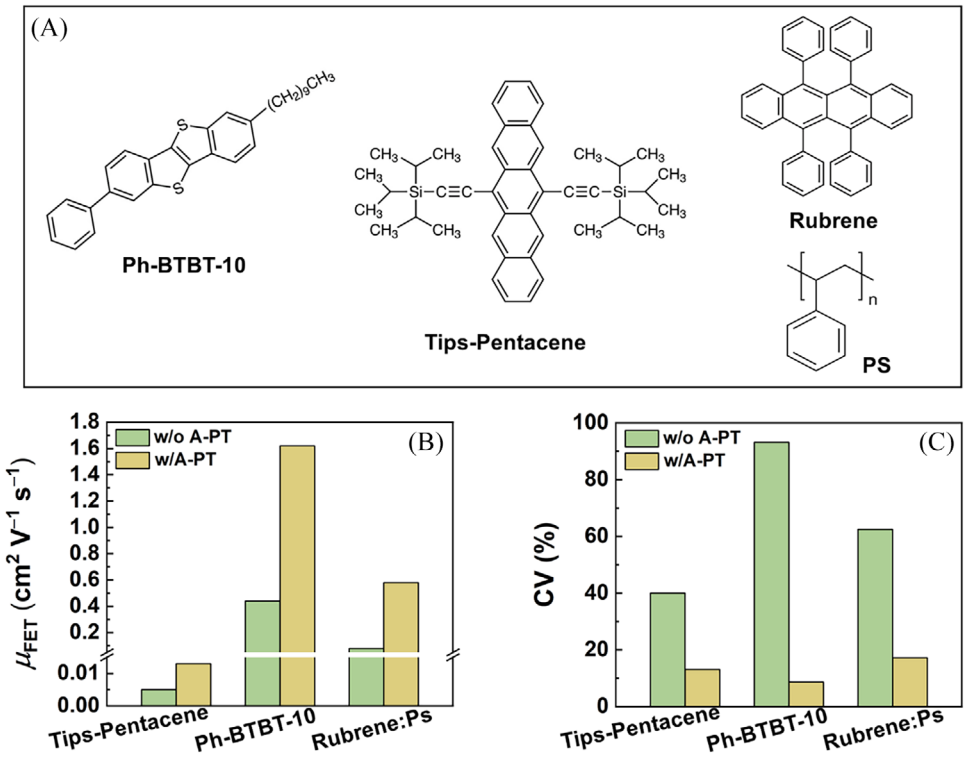

FIGURE 5 (A) Depicts the molecular structures of Ph-BTBT-10, tips-pentacene, rubrene, and PS used in this work to demonstrate the general applicability of the A-PT method for enhancing the operational performance of organic thin-film transistors (OTFTs). Statistical analysis on (B) field-effect mobility (μ_{FET}) and (C) coefficient of variation (CV) in μ_{FET} of the OTFTs with A-PT (w/A-PT) and without A-PT (w/o A-PT).

uniformity of the OTFTs deteriorates exceeding 15 min of annealing time, leading to a decrease in μ_{FET} and an increase in CV for both μ_{FET} and threshold voltage, attributed to the degradation of rubrene film. The above results indicate that although the utilization of A-PT enhances the spreadability of rubrene solution and subsequent high-quality film formation on the substrate, the spontaneous removal of A-PT after spin-coating results in high interface energy between the rubrene film and substrate. Therefore, the rational control of film annealing is essential for optimizing molecule ordering and grain formation, as well as preventing film degradation, in order to achieve optimal electrical uniformity of OTFTs.

To investigate the universal compatibility of A-PT in enhancing the electrical uniformity and other performance aspects of OTFTs, additional widely utilized OSC materials, such as 6,13-bis(triisopropylsilylethynyl)pentacene (Tips-pentacene) and 2-decyl-7-phenyl-[1]benzothieno[3,2-b][1]benzothiophene (Ph-BTBT-10), were employed for device fabrication through the solution spin-coating process, as illustrated in Figure 5A. The transfer curves and corresponding histogram of μ_{FET} for these OTFTs, with and without the use of A-PT, are illustrated in Figure S8. The mean μ_{FET} and CV obtained are plotted in Figure 5B,C. Typically, the utilization of A-PT in the Tips-pentacene OTFTs results in a mean μ_{FET} of 0.013 cm^2 V^{-1} s^{-1} and a CV of 15.4%, whereas devices without A-PT only achieve a mean μ_{FET} of 0.005 cm^2 V^{-1} s^{-1} and a CV of 40.0%. Besides that, the Ph-BTBT-10 OTFTs with A-PT exhibited exceptional electrical properties, demonstrating a mean μ_{FET} of up to 1.62 cm^2 V^{-1} s^{-1} and a maximum μ_{FET} of 1.87 cm^2 V^{-1} s^{-1}, which is nearly four times higher than the μ_{FET} of 0.44 cm^2 V^{-1} s^{-1} obtained from the devices without A-PT. Furthermore, the CV for the Ph-BTBT-10 OTFTs impressively decreased from 93.2% to 8.6% when using A-PT. The device performance of the Ph-BTBT-10 OTFTs fabricated with A-PT surpasses that of previously reported thin-film devices and is even comparable to single-crystal devices. The A-PT was also utilized for the fabrication of OTFTs using a blend of rubrene and PS. The transfer curves and corresponding histogram of μ_{FET} for these OTFTs, with and without the use of A-PT, are illustrated in Figure S9. The mean μ_{FET} was enhanced from 0.08 to 0.58 cm^2 V^{-1} s^{-1} (Figure 5B), while the CV decreased from 62.5% to 17.2% (Figure 5C) in comparison with the performances of the reference devices (Figure 2B,F). The results demonstrate the potential of extending the A-PT method to other OSC materials for fabricating devices with enhanced field-effect mobility and uniform electrical performance.

3 | CONCLUSION

Through utilizing the enhanced wettability of small-molecule solutions on gate oxides via thermally deposited and annealed TPBi-based A-PT, we demonstrated a universal method for fabricating large-area and uniform OSC films by spin-coating small-molecule solutions. Benefiting from the highly ordering alignment of TPBi in the A-PT, the defect-free platelet grains with millimeter-scale domains were formed to promote the formation of uniform OSC films. In addition, the solubility of the annealed TPBi in solvents was effectively reduced, thereby alleviating the detrimental impact of TPBi doping on the performance of OSC film devices. The OTFTs fabricated with the A-PT performed improved field-effect mobility, surpassing those of the OTFTs fabricated by direct spin-coating and polymer blend methods. More importantly,

the OTFTs fabricated with the A-PT demonstrate exceptional device-to-device uniformity, with a 100% device yield, low variation in mobilities within a single-chip array of OTFTs below ~7.7%, and low variation in mobilities across different batches ~12.5%.

4 | EXPERIMENTAL SECTION

Rubrene, Tips-pentacene, and Ph-BTBT-10 were procured from TCI Chemicals Corporation, while TPBi was obtained from Luminance Technology Corporation. PS and 1,2-dichlorobenzene were purchased from Aladdin Corporation. All materials were used as received without further purification. For the solution-based film and device fabrication, Rubrene, Tips-pentacene, and Ph-BTBT-10 were individually dissolved in 1,2-dichlorobenzene at a concentration of 10 mg/mL. To fabricate films and devices, Rubrene was co-dissolved with PS in 1,2-dichlorobenzene at a weight ratio of 4:1 resulting in a concentration of 10 mg/mL.

All OTFTs were fabricated based on heavily doped silicon wafer substrates covered with 300 nm SiO_2. The silicon wafer substrates underwent sequential ultrasonic cleaning in acetone, alcohol, and deionized water followed by nitrogen blow drying. Subsequently, they were subjected to a 30-min treatment of ultraviolet ozone. The cleaned substrates in one batch were directly coated with OCS films by spin-coating OCS solutions at 1500 rpm for 60 s in a nitrogen-filled glove box, followed by annealing at 170°C for 15 min. In another batch, a TPBi PT layer with a thickness of 30 nm was deposited through thermal evaporation at a rate of 1 Å/s using a vacuum evaporation system with a base pressure of approximately 10^{-8} Torr. Subsequently, the obtained TPBi PT-based substrates were annealed at 205°C for 30 min in the glove box. Then, the unannealed and annealed TPBi PT-based substrates were subjected to spin-coating OCS films and annealing treatment, following the identical procedure as described above. Finally, the 100 nm Ag drain/source electrode was deposited at a rate of 2 Å/s by thermal evaporation using a shadow mask. The electrode dimensions are 2000 μm in width and 50 μm in length, respectively. The performance evaluation of OTFTs was conducted using a Keithley 4200 SCS semiconductor parametric analyzer under the default normal test mode in ambient conditions. The field-effect mobility (μ_{FET}) was determined using the following equation, $I_{DS} = (W/2L)\ C_i\ \mu_{FET}\ (V_{GS} - V_{TH})^2$, where L and W represent the length and width of the channel, respectively. C_i denotes the real capacitance of SiO_2. V_{GS} and V_{TH} correspond to the gate voltage and threshold voltage, respectively. The morphology of the films was assessed using a polarized microscope (FJ-3A; Shenzhen Finial Technology Ltd., Co). The molecular orientation of the films was confirmed through variable angle spectroscopic ellipsometry (J.A. Woollam Co., Inc.). The aggregate state of these films was confirmed by the GIXRD (D8 Advance Bruker).

ACKNOWLEDGEMENTS

This work was supported by the National Natural Science Foundation of China [grant Nos. 62164012 and 61904159] and the Applied Basic Research Foundation of Yunnan Province [grant No. 202101AT070025]. We gratefully acknowledge the support from the 2023 Caiyun Postdoctoral Project of Yunnan Province and the Xingdian Talent Plan of Yunnan Province.

CONFLICT OF INTEREST STATEMENT

The authors declare no conflict of interest.

ORCID

Zhenxin Yang https://orcid.org/0009-0009-9244-2490
Jiale Su https://orcid.org/0009-0006-4625-0154
Delong Yang https://orcid.org/0000-0001-8913-3886
Yuhui Liao https://orcid.org/0000-0003-4702-9516

REFERENCES

1. Z. Tian, Z. Zhao, F. Yan, *Wearable Electronics* **2024**, *1*, 1.
2. W. C. Wang, L. F. Chi, *Wearable Electronics* **2024**, *1*, 91.
3. D. Simatos, M. Nikolka, J. Charmet, L. J. Spalek, Z. Toprakcioglu, I. E. Jacobs, I. B. Dimov, G. Schweicher, M. J. Lee, C. M. Fernández-Posada, D. J. Howe, T. A. Hakala, L. W. Y. Roode, V. Pecunia, T. P. Sharp, W. M. Zhang, M. Alsufyani, I. McCulloch, T. P. J. Knowles, H. Sirringhaus, *SmartMat* **2024**, e1291.
4. S. H. Wang, J. Xu, W. C. Wang, G. J. N. Wang, R. Rastak, F. Molina-Lopez, J. W. Chung, S. M. Niu, V. R. Feig, J. Lopez, T. Lei, S. K. Kwon, Y. Kim, A. M. Foudeh, A. Ehrlich, A. Gasperini, Y. Yun, B. Murmann, J. B. H. Tok, Z. A. Bao, *Nature* **2018**, *555*, 83.
5. M. X. Zhang, J. Sun, G. D. Zhao, Y. H. Tong, X. Wang, H. Y. Yu, P. Xue, X. L. Zhao, Q. X. Tang, Y. C. Liu, *Small* **2024**, *20*, 2311527.
6. J. D. Chen, W. F. Zhang, L. P. Wang, G. Yu, *Adv. Mater.* **2023**, *35*, 2210772.
7. G. S. Lee, H. J. Kwon, T. K. An, Y. H. Kim, *Chem. Commun.* **2023**, *59*, 4995.
8. A. F. Paterson, S. Singh, K. J. Fallon, T. Hodsden, Y. Han, B. C. Schroeder, H. Bronstein, M. Heeney, I. McCulloch, T. D. Anthopoulos, *Adv. Mater.* **2018**, *30*, 1801079.
9. C. H. Xu, P. He, J. Liu, A. J. Cui, H. L. Dong, Y. G. Zhen, W. Chen, W. P. Hu, *Angew. Chem. Int. Ed.* **2016**, *55*, 9519.
10. J. Takeya, M. Yamagishi, Y. Tominari, R. Hirahara, Y. Nakazawa, T. Nishikawa, T. Kawase, T. Shimoda, S. Ogawa, *Appl. Phys. Lett.* **2007**, *90*, 102120.
11. H. Minemawari, T. Yamada, H. Matsui, J. Tsutsumi, S. Haas, R. Chiba, R. Kumai, T. Hasegawa, *Nature* **2011**, *475*, 364.
12. X. T. Zhao, H. T. Zhang, J. Zhang, J. Liu, M. Lei, L. Jiang, *Adv. Sci.* **2023**, *10*, 2300483.
13. A. Yamamura, S. Watanabe, M. Uno, M. Mitani, C. Mitsui, J. Tsurumi, N. Isahaya, Y. Kanaoka, T. Okamoto, J. Takeya, *Sci. Adv.* **2018**, *4*, eaao5758.
14. M. R. Niazi, R. P. Li, E. Q. Li, A. R. Kirmani, M. Abdelsamie, Q. X. Wang, W. Y. Pan, M. M. Payne, J. E. Anthony, D. M. Smilgies, S. T. Thoroddsen, E. P. Giannelis, A. Amassian, *Nat. Commun.* **2015**, *6*, 8598.
15. M. Kang, H. Hwang, W. T. Park, D. Khim, J. S. Yeo, Y. Kim, Y. J. Kim, Y. Y. Noh, D. Y. Kim, *ACS Appl. Mater. Interfaces* **2017**, *9*, 2686.
16. P. S. Jo, D. T. Duong, J. Park, R. Sinclair, A. Salleo, *Chem. Mater.* **2015**, *27*, 3979.
17. H. Yoo, H. H. Choi, T. J. Shin, T. Rim, K. Cho, S. Jung, J. J. Kim, *Adv. Funct. Mater.* **2015**, *25*, 3658.
18. Z. W. Zhou, Q. S. Wu, S. J. Wang, Y. T. Huang, H. Guo, S. P. Feng, P. K. L. Chan, *Adv. Sci.* **2019**, *6*, 1900775.
19. H. L. Chen, W. N. Zhang, M. L. Li, G. He, X. F. Guo, *Chem. Rev.* **2020**, *120*, 2879.
20. Q. Y. Sheng, B. Y. Peng, C. Ji, H. Y. Li, *Adv. Mater.* **2023**, *35*, 2304736.
21. M. L. Li, M. Liu, F. Qi, F. R. Lin, A. K. Y. Jen, *Chem. Rev.* **2024**, *124*, 2138.
22. N. Shin, J. Kang, L. J. Richter, V. M. Prabhu, R. J. Kline, D. A. Fischer, D. M. DeLongchamp, M. F. Toney, S. K. Satija, D. J. Gundlach, B. Purushothaman, J. E. Anthony, D. Y. Yoon, *Adv. Funct. Mater.* **2013**, *23*, 366.
23. H. H. Choi, K. Cho, C. D. Frisbie, H. Sirringhaus, V. Podzorov, *Nat. Mater.* **2018**, *17*, 2.
24. T. R. Fielitz, C. M. Phenicie, R. J. Holmes, *Cryst. Growth Des.* **2017**, *17*, 4522.

25. H. W. Lin, C. L. Lin, H. H. Chang, Y. T. Lin, C. C. Wu, Y. M. Chen, R. T. Chen, Y. Y. Chien, K. T. Wong, *J. App. Phys.* **2004**, *95*, 881.
26. S. S. Dalal, D. M. Walters, I. Lyubimov, J. J. de Pablo, M. D. Ediger, *Proc. Natl. Acad. Sci. USA* **2015**, *112*, 4227.
27. H. N. Yang, S. J. He, T. Zhang, J. X. Man, Y. B. Zhao, N. Jiang, D. K. Wang, Z. H. Lu, *Org. Electron.* **2021**, *88*, 106014.
28. S. W. Park, J. M. Hwang, J. M. Choi, D. K. Hwang, M. S. Oh, J. H. Kim, S. Ima, *Appl. Phys. Lett.* **2007**, *90*, 153512.
29. Y. Li, C. Liu, A. Kumatani, P. Darmawan, T. Minari, K. Tsukagoshi, *Org. Electron.* **2012**, *13*, 264.
30. Y. H. Kim, J. E. Anthony, S. K. Park, *Org. Electron.* **2012**, *13*, 1152.
31. S. Sanda, T. Nagase, T. Kobayashi, K. Takimiya, Y. Sadamitsu, H. Naito, *Org. Electron.* **2018**, *58*, 306.
32. S. Sanda, R. Nakamichi, T. Nagase, T. Kobayashi, K. Takimiya, Y. Sadamitsu, H. Naito, *Org. Electron.* **2019**, *69*, 181.
33. F. M. Huang, Y. Xu, Z. C. Pan, W. W. Li, J. H. Chu, *IEEE Electron Device Lett*. **2020**, *41*, 1082.
34. H. Ren, N. Cui, Q. X. Tang, Y. H. Tong, X. L. Zhao, Y. C. Liu, *Small* **2018**, *14*, 1801020.
35. S. Y. Wang, X. L. Zhao, Y. H. Tong, Q. X. Tang, Y. C. Liu, *Adv. Mater. Interfaces* **2020**, *7*, 1901950.
36. Z. Chen, S. M. Duan, X. T. Zhang, B. W. Geng, Y. L. Xiao, J. S. Jie, H. L. Dong, L. Q. Li, W. P. Hu, *Adv. Mater.* **2022**, *34*, 2104166.
37. W. Deng, H. M. Lei, X. J. Zhang, F. M. Sheng, J. L. Shi, X. L. Zhang, X. Y. Liu, S. Grigorian, X. H. Zhang, J. S. Jie, *Adv. Mater.* **2022**, *34*, 2109818.
38. J. W. Wang, Z. Ren, J. Pan, X. F. Wu, J. S. Jie, X. H. Zhang, X. J. Zhang, *Adv. Mater.* **2023**, *35*, 2301017.
39. S. Y. Yoon, N. Young, P. J. van der Zaag, D. McCulloch, *IEEE Electron Device Lett*. **2003**, *24*, 22.
40. H. Kuriyama, T. Kuwahara, S. Ishida, T. Nohda, K. Sano, H. Iwata, S. Noguchi, S. Kiyama, S. Tsuda, S. Nakano, M. Osumi, Y. Kuwano, *Jpn. J. Appl. Phys. Part 1 Regul. Pap. Short Notes Rev. Pap.* **1992**, *31*, 4550.
41. S. S. Lee, S. Muralidharan, A. R. Woll, M. A. Loth, Z. Li, J. E. Anthony, M. Haataja, Y. L. Loo, *Chem. Mater.* **2012**, *24*, 2920.

SUPPORTING INFORMATION

Additional supporting information can be found online in the Supporting Information section at the end of this article.

How to cite this article: Z. Yang, J. Su, J. Wang, X. Li, F. Li, J. Hu, N. Chen, Z. Tao, D. Yang, D.-K. Wang, Q. Zhu, Y. Liao, Z.-H. Lu, *Aggregate* **2024**, e661. https://doi.org/10.1002/agt2.661